Robotica (2009) volume 27, pp. 389–402. © 2008 Cambridge University Press
doi:10.1017/S0263574708004803 Printed in the United Kingdom

Improving the stability level for on-line planning of mobile manipulators

Changwu Qiu†*, Qixin Cao‡, Leibin Yu† and Shouhong Miao†

†*School of Mechanical Engineering, Shanghai Jiao Tong University, Shanghai, China.*
‡*State Key Laboratory of Mechanical System and Vibration, Shanghai Jiao Tong University, Shanghai, China.*

(Received in Final Form: June 2, 2008. First published online: July 9, 2008)

SUMMARY
This paper presents a quadratic programming (QP) form algorithm to realize on-line planning of mobile manipulators with consideration for improving the stability level. With Lie group and screw tools, the general tree topology structure mobile robot dynamics and dynamic stability attributes were analysed. The stable support condition for a mobile robot is constructed not only in a polygonal support region, but also in a polyhedral support region. For a planar supporting region, the tip-over avoiding requirement is formulated as the tip-over prevent constraints with the reciprocal products of the resultant support wrench and the imaginary tip-over twists, which are constructed with the boundaries of the convex support polygon. At velocity level, the optimized resolution algorithm with standard QP form is designed to resolve the inverse redundant kinematics of the Omni-directional Mobile ManipulatorS (OMMS) with stability considerations. Numerical simulation results show that the presented methods successfully improve the stability level of the robot within an on-line planning process.

KEYWORDS: Mobile manipulator; Stability; Tip-over avoiding; On-line planning; Inverse redundant kinematics.

1. Introduction

The dual-arm mobile robot has an advantage to be an assistant or to take the place of humans to work in an environment with the interface for a human being. The mobility endows the robot great versatility and flexibility. However, the mobile robot is a structurally unstable system; it has a possibility of overturning under the dynamic wrench action caused by inertial or outside forces arising from manipulation or disturbance. It is particularly prone to tip-over for robots with small-sized mobile platforms, which is a necessary condition for applications in homes, offices or workshops. Keeping support stability is an important premise to finish manipulation tasks for mobile robots. On the other hand, the working environment is commonly an unstructured environment. Therefore, on-line tip-over avoidance ability must be considered in a mobile manipulator's control system design. In this paper, we focus on the study of the dynamic stability and the on-line planning method with improving stability considerations for a service robot with an Omni-directional Mobile ManipulatorS (OMMS) configuration.

Some profound comparative analysis and new stability measures for static or dynamic stability have been presented and proposed in previous works.[1–4] Rey and Papadopoulos[5] have proposed the force-angle measure for the tip-over stability prediction and prevention algorithm for a mobile manipulator. Abo-Shanab and Sepehri[6] took a Caterpillar 215B excavator-based log-loader as the prototype; they modelled and simulated the dynamic stability behaviour during aback-and-forth motion of the base. Huang *et al.*[7] have proposed a stability control method based on the simplified ZMP (zero moment point) criterion, which neglects the mass moment of rigid bodies. They separated the system into vehicle and manipulator parts and utilized only the manipulator motion to compensate the system stability. However, the strong dynamic interaction makes the combined scheme better than the separated one.[8] Furuno *et al.*[9] formulated the distance from the simplified ZMP to the boundary of the stable support region to be a nonlinear inequality constraint and then combined the constraints to be an optimal control problem. The hierarchical gradient method was used to solve the problem. However, the method is weak in treating a dynamic environment and has less efficiency. Li and Liu[10] presented a new on-line overturn prevention algorithm to optimize the supporting force distribution on wheels by controlling self-motions of the on-board redundant mobile manipulator. Wieber[11] presented a profound analysis about the dynamic stability of the walking system and proposed a new stability margin definition with the Lyapunov sense.

Mobile platform endows the manipulator(s) system extra degrees of freedom, which largely extend the workspace and the ability of the robot to work in dynamic environment. Most of the research works modelled the kinematics and dynamics of the manipulator(s) in global coordinates,[1–10] which require updating accurate position/pose information of the system in microseconds. In unstructured environments and field applications, global position/pose information needs extra sensor devices; moreover, that is arduous and mistakable to detect with respect to the precision and real-time demands. However, replacing the reference inertial frame with a local one and determining the attitude of the

* Corresponding author. E-mail: qcw@sjtu.org

system with proprioceptive sensors is a convenient way for task fulfillment. For example, we unconsciously locate the cup relative to the table but not to the frame of the door when we try to fetch the cup on the table. In this paper, we will implement the dynamics and stability analysis with left invariant form to make the formulation of the kinematics and dynamics of the system self-reliant. In Sections 2 and 3, we will show that it is enough to treat the stability and dynamics of the system with the proprioceptive attitude information and the configuration information of the body-fixed frame to an arbitrary inertial frame.

When a mobile robot is moving on a given terrain, the system states space can be split into two subspaces: one can fulfill the system motion without tip-over, and the other cannot avoid tip-over to fulfill the system motion.[11] The two subspaces of the system states space can be formulated as inequality constraints for the system states. In this paper, the tip-over prevent constraints (TPC) and joint motion constraints (JMC), which are constructed from joint range, velocity and acceleration limits, are formulated as unified linear inequality constraints at velocity level. The task equality constraints, TPC and JMC are incorporated into standard quadratic programming (QP) method to resolve the on-line planning of a dual-arm mobile robot with dynamic stability consideration.

This paper is organized as follows. Section 2 presents the OMMS robot system description and the general dynamics modelling method for the tree topology mobile robot. Section 3 presents the generalized stable support condition for mobile robot, the new stability optimization criteria and the TPC. In Section 4, we incorporate the task equality constraints, JMC and TPC into the standard QP algorithm to realize on-line path planning with consideration for improving the stability level. In Section 5, simulation results of the proposed method are presented to exhibit the effectiveness of the proposed method. Conclusions are summarized in Section 6.

2. System Dynamics

2.1. OMMS system description

The prototype of the OMMS system is shown in Fig. 1. The coordinate frames configuration of the OMMS system is shown in Fig. 2. The system consists of three subsystems: one omni-directional mobile platform and two individual 7-DOF spatial manipulators. In Fig. 2, the mobile platform is depicted as a trunk rigidly mounted on a triangular plate and is connected with revolute joints to three independent driving Mekanum wheels, which are symmetrically configured and consist of a number of free-spinning castor wheels positioned on the periphery of the wheel circumference and allowed for near-friction-free movement parallel to the Mekanum wheel's axes of rotation. The omni-directional mobile platform endows the robot with the holonomic mobility on plane. The label in Fig. 1 shows the prototype of the Mekanum wheel in this work. We denote the wheel, the trunk and the left and right manipulators with subscripts 'w', 'c', 'l' and 'r', respectively.

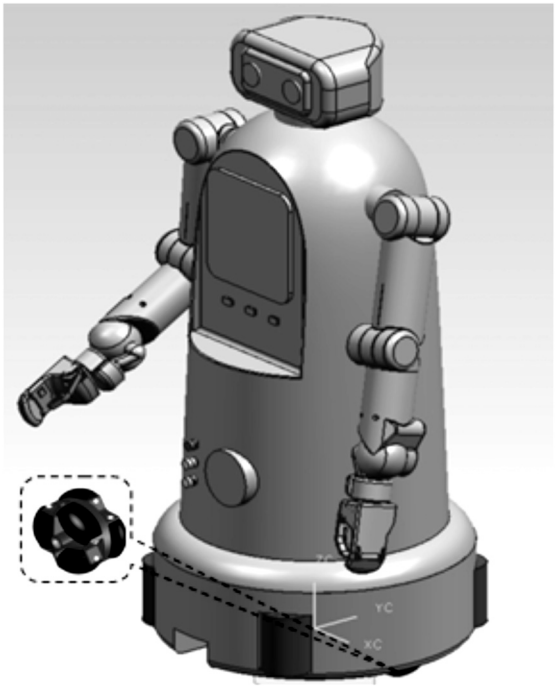

Fig. 1. The omni-directional dual arm service robot prototype.

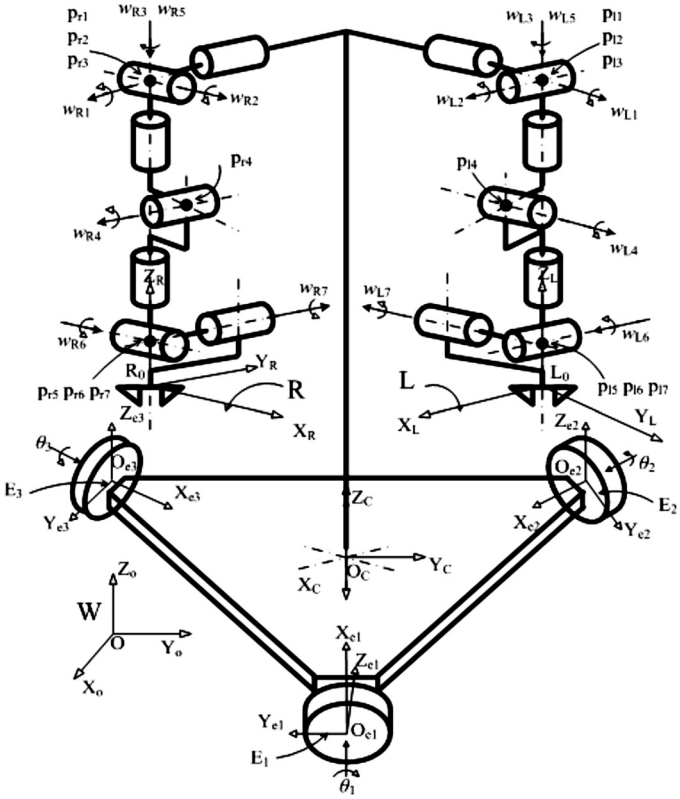

Fig. 2. Coordinate frames for the OMMS system.

Most mobile robots are tree topology structure systems and hence have superior dexterity and adaptability. The presented prototype is of a tree topology structure mechanism also. We describe the motion of the robot bodies using the twist and product-of-exponential (POE) formula. The initial twist parameter of the joints is calculated with respect to the

body-fixed coordinate frame $C(O_c - X_cY_cZ_c)$ located on the trunk, which is the root body of the tree structure multi-body system. In view of the wide space mobility of the mobile robot, we adopt the left invariant body screw coordinates to model the system with self-reliant style. (In fact, the screw motion is expressed in an instantaneous imaginary inertia frame that superposes with the body-fixed frame. In this work, we obey the notation habits[12] and name this image frame as body-fixed coordinate frame.)

2.2. Dynamics of the system

In this section, the OMMS system dynamics is modelled with geometry view and better schematic based on the theory of Lie groups and screw. Geometry background for the rigid body motion and force wrench is not expatiated repeatedly for the length consideration. (Refer to the works of Murray *et al.*[12] and Park *et al.*[13] for detailed background information.)

We take the tree topology as the general structure to model the OMMS system dynamics and do not refer to the other mobile robot type. Choosing arbitrarily a body-fixed frame ${}^j\mathrm{B}_i$ for the body i of the branch j, the configuration, velocity and acceleration of the body are

$$g_{ji} = g_{wc}e^{\hat{\xi}_{j1}q_{j1}} \cdots e^{\hat{\xi}_{ji}q_{ji}} g_{c,ji}(0), \tag{1}$$

$$V_{ji} = \left(g_{ji}^{-1}\dot{g}_{ji}\right)^{\vee} = Ad_{g_{c,ji}^{-1}} V_c + J_{ji}\dot{q}_j, \tag{2}$$

$$\dot{V}_{ji} = Ad_{g_{c,ji}^{-1}(0)}({}^jT_{i1}V_c)' + J_{ji}\ddot{q}_j + \dot{J}_{ji}\dot{q}_j, \tag{3}$$

where $g_{wc} \in SE(3)$ is the configuration of the frame C respect to the chosen inertial reference frame W, $g_{c,ji}(0) \in SE(3)$ is the initial configuration of the j-th branch's i-th body-fixed frame ${}^j\mathrm{B}_i$ respect to the frame C, and $g_{c,ji} = g_{wc}^{-1}g_{ji}$ is the current configuration of the j-th branch's i-th body-fixed frame respect to the frame $C \cdot \xi_{ji} = [-w_{ji} \times p_{ji}, w_{ji}]^T \in R^6$ is the twist of the i-th joint axis of the j-th branch respect to the frame C, where w_{ji} is the unit vector in the direction of the joint axis and p_{ji} is an arbitrary point on the axis of the joint $i \cdot V_c = (g_{wc}^{-1}\dot{g}_{wc})^{\vee} \in R^6$ is the body twist of the frame C. In view of the attributes of the left invariant presentation, V_c will not change when the inertial reference coordinate frame is altered. $q_j = [q_{j1}, \ldots, q_{jm}]^T \in R^m$ is the joint variable of the branch $j \cdot J_{ji}$ is the body Jacobian matrix of the i-th body in j-th branch and has the form

$$J_{ji} = Ad_{g_{c,ji}^{-1}(0)}[{}^jT_{1i}\xi_{j1}, \ldots, {}^jT_{ii}\xi_{ji}, 0, \ldots, 0] \in R^{6\times m}, \tag{4}$$

where $Ad_g \in R^{6\times 6}$ is the adjoint transformation associated with g. The matrix ${}^jT_{ik} \in R^{6\times 6}$ has the form

$${}^jT_{ki} = \begin{cases} Ad_{(e^{\hat{\xi}_k q_k}e^{\hat{\xi}_{k+1}q_{k+1}}\ldots e^{\hat{\xi}_i q_i})^{-1}} & i > k, \\ I_6 & i = k, \\ 0 & i < k. \end{cases} \tag{5}$$

The differential form of the adjoint transformation of a twist $V \in R^6$ is

$$\begin{aligned}(T_{ij}V)' &= T_{ij}\dot{V} + \sum_{k=i+1}^{j} T_{kj}[T_{i,k-1}V, \xi_k]\dot{q}_k \\ &= T_{ij}\dot{V} + \sum_{k=i+1}^{j} T_{kj}ad_{T_{i,k-1}V}\xi_k\dot{q}_{l_k},\end{aligned} \tag{6}$$

where $ad_{\xi_1}\xi_2$ is the adjoint representation of the Lie bracket $[\xi_1, \xi_2]$.

For a rigid body with twist in the body-fixed frame, the Newton–Euler equation has the form[12]

$$M\dot{V} - ad_V^T MV = F, \tag{7}$$

where $M \in R^{6\times 6}$ is the generalized inertial matrix of the rigid body, $V \in R^{6\times 1}$ is the body twist of the rigid body and $F \in R^{6\times 1}$ is the external wrench applied on the rigid body and consists of gravitational force and external force. All these terms are expressed with respect to a same body-fixed frame.

Based on the d'Alembert principle, we define the inertial wrench as $F^I = M\dot{V} - ad_V^T MV$. Combining the property that the reciprocal product of twist and wrench gives the instantaneous power, and Jourdain's variation principle, we can get the equation

$$(F - F^I) \cdot \delta V = 0. \tag{8}$$

Extending the above equation to multi-rigid body systems,

$$\sum_{i=1}^{n} \left(F_i + R_i - F_i^I\right) \cdot \delta V_i = \sum_{i=1}^{n} R_i \cdot \delta V_i = 0, \tag{9}$$

where F_i is the generalized external wrench (including active driving force/torque, gravity force and external wrenches acted on by environment) applied on body i, R_i is the ideal constraint wrench applied on body i and F_i^I is the inertial wrench of body i (each term is expressed with respect to the i-th body-fixed coordinate frame). For further simplification, we decompose the generalized external wrench F_i into active driving wrench F_i^A, dissipation wrench F_i^{φ} and the external wrench F_i^E. Equation (9) can be rewritten as

$$\sum_{i=1}^{n} \left(F_i^A + F_i^E + F_i^{\varphi} - F_i^I\right) \cdot \delta V_i = 0. \tag{10}$$

Assuming that the joint velocity is $\dot{q} = [\dot{q}_1, \dot{q}_2, \ldots, \dot{q}_n]^T \in R^{n\times 1}$ and all joints are actively driven, the driving torque/force is τ_i and the dissipation torque/force is φ_i, the system dynamics equation of the OMMS system can be

written as

$$\sum_{i=1}^{n}\left(\tau_i\cdot\delta\dot{q}_i+\varphi_i\cdot\delta\dot{q}_i+F_i^E\cdot\delta V_i-F_i^I\cdot\delta V_i\right)+F_c^E\cdot\delta V_c-F_c^I\cdot\delta V_c=0. \tag{11}$$

According to Eq. (11) and considering the independent property of the variation of the generalized coordinates, the OMMS system dynamics can be modelled as a canonical form,

$$J^T(F^I-F^E)=\tau+\varphi, \tag{12}$$

where $F^I=[(F_c^I)^T,(F_w^I)^T,(F_l^I)^T,(F_r^I)^T]^T$, $F^E=[(F_c^E)^T,(F_w^E)^T,(F_l^E)^T,(F_r^E)^T]^T$,

$$J=\begin{bmatrix} I_6 & & & 0\\ A_w & J_w & & \\ A_l & 0 & J_l & \\ A_r & 0 & 0 & J_r\end{bmatrix}\in R^{108\times 23},$$

$$A_w=\begin{bmatrix} Ad_{g_{c,w1}^{-1}}\\ Ad_{g_{c,w2}^{-1}}\\ Ad_{g_{c,w3}^{-1}}\end{bmatrix}\in R^{18\times 6},$$

$$A_l=\begin{bmatrix} Ad_{g_{c,l1}^{-1}}\\ \vdots\\ Ad_{g_{c,l7}^{-1}}\end{bmatrix}\in R^{42\times 6},$$

$$A_l=\begin{bmatrix} Ad_{g_{c,r1}^{-1}}\\ \vdots\\ Ad_{g_{c,r7}^{-1}}\end{bmatrix}\in R^{42\times 6},$$

$$J_w=\begin{bmatrix} Ad_{g_{c,w1}^{-1}(0)}\xi_{w1} & & 0\\ & Ad_{g_{c,w2}^{-1}(0)}\xi_{w2} & \\ 0 & & Ad_{g_{c,w3}^{-1}(0)}\xi_{w3}\end{bmatrix}\in R^{18\times 3},$$

$$J_l=\begin{bmatrix} J_{l1}\\ J_{l2}\\ \vdots\\ J_{l7}\end{bmatrix}\in R^{42\times 7},\quad J_r=\begin{bmatrix} J_{r1}\\ J_{r2}\\ \vdots\\ J_{r7}\end{bmatrix}\in R^{42\times 7},$$

$$\tau=\begin{bmatrix} 0\\ \tau_w\\ \tau_l\\ \tau_r\end{bmatrix}\in R^{23\times 1},\quad \varphi=\begin{bmatrix} 0\\ \varphi_w\\ \varphi_l\\ \varphi_r\end{bmatrix}\in R^{23\times 1}.$$

Note that Eq. (11) gives the general OMMS system dynamics model. For the first six equations, there are no actuation forces. The trunk's motion realization must depend on appropriate actuation of each joint and contact forces transformed from wheels. However, if the robot moves on a plane, and there is no tip-over and slippage between wheels and the floor, the system dynamics model will not include the independent part for the trunk, and there exists a relation $V_c=P\dot{q}_w$, where $q_w\in R^3$ is the wheel rotation angle and $P\in R^{6\times 3}$ is constant and decided by structure parameters.

In Eq. (11), the term F^E includes the gravity forces F^G and contact forces F^C arising from contact with environment. Assuming that there have been contact forces only in the wheel and floor touching area, we neglect the dissipation force action and substitute the inertial wrench into (12); the system dynamics has the form

$$\begin{bmatrix} M_1\\ M_2\end{bmatrix}\begin{bmatrix}\dot{V}_c\\ \ddot{q}\end{bmatrix}+\begin{bmatrix} C_1\\ C_2\end{bmatrix}\begin{bmatrix} V_c\\ \dot{q}\end{bmatrix}+\begin{bmatrix} G_c\\ G_q\end{bmatrix}=\begin{bmatrix} 0\\ T\end{bmatrix}+\begin{bmatrix} A_w^TF_w^C\\ F_q^E\end{bmatrix}, \tag{13}$$

where $q=[q_w^T,q_l^T,q_r^T]^T\in R^{17\times 1}$ is the joint variable vector of the OMMS system, $T=[\tau_w^T,\tau_l^T,\tau_r^T]\in R^{17\times 1}$ is the actuation torque vector of the OMMS system and $G_c\in R^{6\times 1}$ and $G_q\in R^{17\times 1}$ are the system gravity force actions for the trunk and the other links respectively. $F_w^C\in R^{18\times 1}$ is the contact wrench vector acted on wheel by floor and descript in the wheel body-fixed frame. $F_q^E=[J_w^TF_w^C,0,0]\in R^{17\times 1}$ is the contact force action in joint space. Other details are omitted for length consideration.

Assuming the wheel floor contact is of the point contact type. The local contact frame is shown in Fig. 3(a). In each contact point, there exist contact forces $f_i=[f_x^i,\ f_y^i,\ f_z^i]^T, i=1,\ 2,\ 3,\ f_z^i$, and $[f_x^i,f_y^i]^T$ are the normal and tangential components of the contact forces respectively. According to Coulomb's law and considering the unilateral constraints, there exist inequality constraints as

$$\begin{cases} f_z\geq 0\\ \mu f_z\geq\sqrt{f_x^2+f_y^2}\end{cases}. \tag{14}$$

Let $B_i\in R^{6\times 3}$ be the transformation matrix to transform the contact forces from the contact frames to the wheel body-fixed frame. We can obtain F_w^C as

$$F_w^C=\begin{bmatrix} B_1f_1\\ B_2f_2\\ B_3f_3\end{bmatrix}. \tag{15}$$

Combining (13), (14) and (15), we can get the realizable system motion dynamics equation. Analysing the above equations, we can find the necessary condition for a mobile robot to realize a given movement as there exist contact forces satisfying (14) when the actuation forces are applied to the dynamics system modelled with (13). However, keeping support stable is another important necessary condition to realize desirable motion or manipulation for a mobile robot.

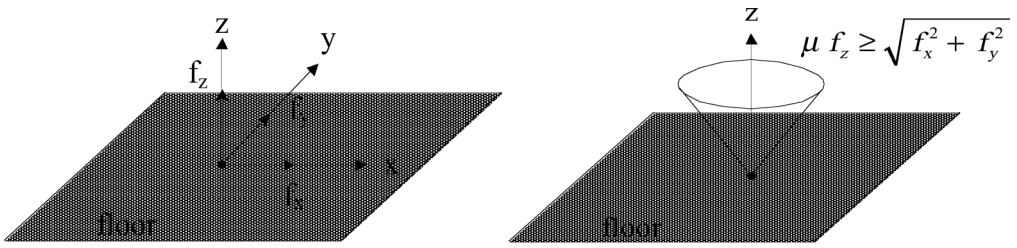

(a) (b)

Fig. 3. The contact force is expressed as three components in (a), the contact force vector is limited within the Coulomb's friction cone as shown in (b).

In the following section, the dynamic stable support condition for a mobile robot will be analysed.

3. Dynamic Stability Constraints

Section 2 has presented the general dynamic model method with Lie group tools for the tree topology structure of a mobile robot. The necessary condition for realizable movement of the robot is summarized in Eqs. (13) and (14). We found that the movement of the robot strongly relies on the available contact forces and the appropriate driving forces. Based on this observation, the stability of the mobile robot can be defined as to keep contact status unchanged and to provide the support for the movement and pose transformation of the robot system with appropriate driving forces. Keeping contact status unchanged has two aspects: one is for avoiding tip-over, the other is for avoiding slippage.

In this work, stable support is defined as that in which the relative acceleration in the tangential direction of the contacting surface between the mobile robot and the ground is zero. The situation for tip-over or accelerated sliding motion between the mobile robot and the supporting ground is defined as unstable support. In applications, a tip-over is more dangerous than a slippage. Avoiding slippage requires more effort to have the robot system comply with the environment than does avoiding tip-over; it needs detailed information on the attributes of the local terrain contacted with the robot. In this section, we will focus only on the tip-over avoiding principle.

3.1. Generalized condition for stable support

At any instantaneous time, there exists wrench equilibrium equation in the arbitrarily chosen body-fixed frame for the inertial wrench and the external wrench acted on the mobile robot system. The external wrench includes the gravity forces and the contact forces acted on the mobile robot system by environment. The equilibrium equation has the form

$$F^I - F^G - F^M = F^S, \tag{16}$$

where $F^I \in R^6$, $F^G \in R^6$, $Ft^S \in R^6$ and $F^M \in R^6$ are the resultant inertial wrench (RIW), the resultant gravity wrench (RGW), the resultant supporting wrench (RSW) and the resultant reaction manipulation wrench (RRMW) for the robot system respectively. Here, the contact wrenches acted on the robot by environment are differentiated as RSW and RRMW according to whether the contact wrenches are for supporting action. In this work, we define the left part of (16) as the *dynamic load wrench* of the mobile robot, the definition of which is as follows:

For a mobile robot, the sum of the resultant inertial wrench, negative resultant gravity wrench and negative resultant reaction manipulation wrench except contact wrenches for supporting action is called the dynamic load wrench of the mobile robot system.

Assuming Eq. (16) is set up in frame C fixed on the root body of the tree topology structure system, the RIW, RGW and RRMW have the forms

$$F^I = F_C^I + \sum_{i,j} Ad^T_{g^{-1}_{c,ji}} F^I_{ji}, \tag{17}$$

$$F^G = F_C^G + \sum_{i,j} Ad^T_{g^{-1}_{c,ji}} F^G_{ji}, \tag{18}$$

$$F^M = F_C^M + \sum_{i,j} Ad^T_{g^{-1}_{c,ji}} F^M_{ji}, \tag{19}$$

where F_C^I, F_C^G and F_C^M are the inertial, gravity and reaction manipulation wrenches for the root body in C respectively; F^I_{ji}, F^G_{ji} and F^M_{ji} are the inertial, gravity and reaction manipulation wrenches of j-th branch's i-th body in frame ${}^j\mathrm{B}_i$ respectively; and $g_{c,ji}$ is the configuration of the j-th branch's i-th body-fixed frame ${}^j\mathrm{B}_i$ respect to the frame C.

The RSW is passive and cannot be controlled directly. So we can make the system avoid tip-over only by adjusting RIW, RGW and RRMW. For a mobile robot, the effective support region may be approximated with convex polygon or convex polyhedron (shown in Fig. 4). For the planar supporting situation, the well-known ZMP[14]-based tip-over prevent criterion is often applied in avoiding tip-over of the mobile robot.[7,9,14–16] The assumption of the rigidity of the flat ground, which can provide arbitrary normal contact forces passively induced by the dynamic load wrench of the mobile robot system, is the important premise for the ZMP criterion. According to the ZMP criterion, the tip-over possibility of the mobile robot can be judged by whether the intersection point of the supporting plane and the line of equivalent force corresponding to the dynamic load wrench of the robot system is an inner point of the convex support polygon. When the supporting region is not a

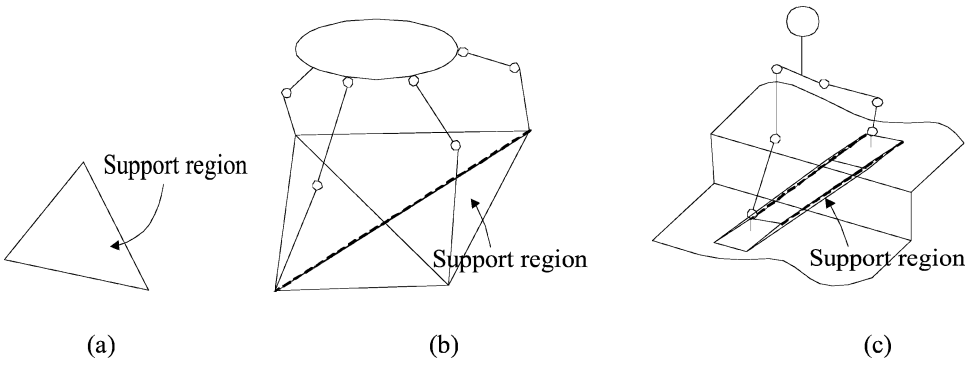

Fig. 4. Different support regions for different robots: (a) The planar support polygon for a mobile robot walking on a plane terrain; (b) The support polyhedron for quadruped robot walking on uneven terrain; (c) The support polyhedron for a biped robot stepping up the stairs.

planar one, the supporting stability condition is complicated. The force-closure concept[12] usually used in grasp stability judgement for multi-fingered hands can be referred to set up the definition for the stable supporting condition of a mobile robot with arbitrary supporting region (including polygon and polyhedron supporting region) as shown in Fig. 4. For a planar support situation, if the induced constrained forces arising from supporting points can resist any perturbation torque which parallels the supporting plane, we say that the support for the mobile robot is stable. Similar conclusion can be deduced for a polyhedron supporting situation, where the polyhedron is decomposed as polygons. We can summarize the following proposition.

Stable support for a mobile robot: A mobile robot has stable support if and only if the induced resultant supporting wrench can resist any perturbation torque which causes a tumbling action for the supporting polygon or polyhedron.

For the planar stable supporting situation, we can choose the objective supporting plane (OSP) (where the support polygon is laid on) as shown in Fig. 5. The equation of the plane in the body-fixed frame C is expressed as $a(x - x_0) + b(y - y_0) + c(z - z_0) = 0$. $p_0 = [x_0, y_0, z_0]^T$ is any point on the OSP. At the coordinate frame Z, where the origin is the ZMP located on the OSP and its z-axis parallels with the normal vector of the OSP, the transformed RSW can be expressed as

$$F_z^{\mathrm{S}} = Ad_{g_{CZ}}^T F^{\mathrm{S}}, \tag{20}$$

where $g_{CZ} = (p, R) \in SE(3)$ is the configuration of the frame Z to the frame C, F^{S} has the vector form $[f^T, \tau^T]^T$, $f = [f_1, f_2, f_3]^T \in R^3$ and $\tau = [\tau_1, \tau_2, \tau_3]^T \in R^3$. The ZMP balance condition requires that the wrench F_Z has no moment component along the OSP,[14] and hence we can conclude that the vector $\tau - \widehat{p} f$ is parallel with the normal vector of the OSP. Combining the OSP equations, the ZMP on the OSP can be resolved from

$$p_{\mathrm{ZMP}} = \begin{cases} a(x - x_0) + b(y - y_0) + c(z - z_0) = 0 \\ (\tau - \widehat{p} f)//[a, b, c]^T \end{cases}. \tag{21}$$

Here, we do not present the analytical form of (21) considering that the equation group must be adjusted according to the different component forms of the OSP's

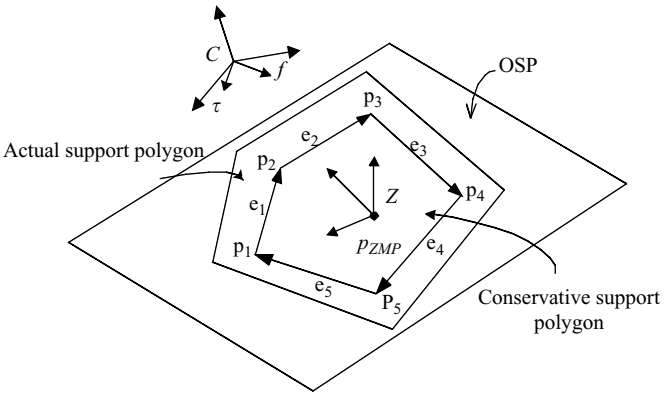

Fig. 5. The relation of the Objective Support Plane (OSP), the Actual Support Polygon (CSP) and the Conservative Support Polygon (CSP).

normal vector. The configuration of the supporting region with respect to the chosen body-fixed frame is deduced only from the joint variables and the contact status information. Therefore the presented method is self-reliant and more realizable than that set up in a global coordinates frame.

In this work, we focus only on the situation in which the OMMS system moves on a plane. In the OSP shown in Fig. 5, the actual support polygon (ASP) is the section of the support region superposed with the OSP. When the ZMP exists within the domain of the ASP, the robot will keep its support balance from tip-over. Let S_{ASP} represent the point set of the ASP. The ZMP criterion can be expressed as

$$p_{\mathrm{ZMP}} \in S_{\mathrm{ASP}}. \tag{22}$$

In literatures for biped locomotion,[14,15] avoiding tip-over is often realized with the path following the desired ZMP trajectory. This method applies strong constraints to the system dynamic motion except the task constraints. The tradeoff between constraints, energy consumption consideration and manipulation action will make the desired ZMP path following fail easily.[16] We can lose the balance constraints by making the ZMP locate in a conservative support region, represented with a conservative support polygon (CSP) as shown in Fig. 5, instead of limiting the ZMP to a desired path. In the next subsection, we will

formulate this idea as a group of inequality constraints at velocity level.

3.2. Tip-over prevent constraints

At any instantaneous time, the robot will not tip-over or loose support when the ZMP is located in the ASP for a planar stable support situation. If the ZMP is located on the boundary of the ASP, the robot system will be prone to tip-over under perturbations. For increasing the robustness and the level of the support stability, we choose a subset of ASP, shown as CSP in Fig. 5, as the feasible range for the ZMP. As shown in Fig. 5, we construct an imaginary twist with the point p_i and the vector e_i as $\xi_i = [-(e_i \times p_i)^T, e_i^T]^T$ in frame C. Assuming the criterion $p_{\mathrm{ZMP}} \in S_{\mathrm{CSP}}$ is satisfied, it means that the RSW, F^{S}, will generate negative power as the robot moves with the twist ξ_i. Therefore, we can construct TPCs as

$$\xi_i^T F^{\mathrm{S}} \leq 0. \tag{23}$$

When the TPCs are satisfied, the dynamic power stability margin can be defined as the smallest instantaneous perturbation power to tumble the robot around one edge of the CSP, that is,

$$\operatorname*{Max}_i(F^{\mathrm{S}} \cdot \xi_i). \tag{24}$$

Then we can construct the optimization criterion to improve the stability level as

$$\mathrm{Min}(\max_i(F^{\mathrm{S}} \cdot \xi_i)). \tag{25}$$

The optimization criterion (25) is more effective than the constraints (23) in improving the stability level for avoiding tip-over. However, the above criterion cannot assure that the TPC is not broken in the task execution process. So we must apply the TPC to confine the system states out of the subspace which will cause a tip-over motion of the system. How to deal with the improving stability requirement and avoiding tip-over simultaneously is our concern.

Because of the mobility of the platform and the redundant manipulator design, the OMMS system is a redundant system. The QP algorithm has been proved as an effective way to resolve the redundancy problem.[17] At velocity level, we can transform the TPC to be inequality constraints of a unified form with the JMC, which are constructed from joint range, velocity and acceleration limits. Then, the TPC and the JMC can be incorporated into standard QP algorithm to resolve the redundancy problem. At acceleration level, the TPC for the OMMS system has the following linear form:

$$\xi_i^T(F^I - F^G - F^M) \leq 0. \tag{26}$$

Considering the need to alleviate computation load, we can transform the above constraints from the second-order level to the first-order level of system states according to the difference relation $\ddot{q}(t - \Delta t) = (\dot{q}(t) - \dot{q}(t - \Delta t))/\Delta t$. The TPC at velocity level has the form

$${}^j A_T(q(t - \Delta t))\dot{q}(t) \leq {}^j B_T(q(t - \Delta t)), \tag{27}$$

where $\dot{q}(t) = [V_C^T(t), \dot{q}_l^T(t), \dot{q}_r^T(t)]^T \in R^{20}$, ${}^j A_T(q(t - \Delta t)) \in R^{1\times 20}$ and ${}^j B_T(q(t - \Delta t)) \in R$ are set up for the j-th twist ξ_j, which corresponds to the edge of the CSP. The details can be found in the appendix.

For the simplest situation in which the robot moves with no slippage on a plane, the trunk's twist motion can be conveniently realized with the driving wheels. The relation between the wheel rotation velocity and the body twist of the trunk can be deduced as $V_c = P\dot{q}_w$, where $q_w \in R^3$ is the wheel rotation angle and $P \in R^{6\times 3}$ is constant and decided by structure parameters. Therefore, the velocity of the system states will be $\dot{q}(t) = [\dot{q}_w^T(t), \dot{q}_l^T(t), \dot{q}_r^T(t)]^T \in R^{17}$. When slippage cases occur, the trunk's motion cannot be controlled directly. In such situations, the trunk's dynamic wrench action can be treated as a part of ${}^j B_T$ and the velocity of the system states in (27) can be chosen as $\dot{q}(t) = [\dot{q}_l^T(t), \dot{q}_r^T(t)]^T \in R^{14}$.

4. Optimized Planning

The OMMS system is a redundant DOF system. At velocity level, the optimized solution under equality and inequality constraints for the inverse redundant kinematics (IRK) can be got with optimized solution as

$$\text{Minimize } H(q, \dot{q}), \tag{28}$$

$$\text{Subject to } J\dot{q} = \dot{x}, \tag{29}$$

$$A\dot{q} \leq B, \tag{30}$$

where $H(q, \dot{q}) \in R$ is a performance function. Equation (29) represents the relationship between the end-effector velocity and the joint velocity. The function $H(q, \dot{q})$ can be linear or nonlinear in form. Because of the consistency attribute of system dynamics, the quadratic form's performance function is preferred, such as $H(q, \dot{q}) = \frac{1}{2}\dot{q}^T W\dot{q} + \varphi\dot{q}$, where $W(q) \in R^{m\times m}$ is a positive definite cost matrix and $\varphi(q) \in R^{1\times m}$ is a linear cost vector. The natural choice of the performance function for (28) is the minimized system kinetic energy. For simplifying the algorithm realization, we choose the const weighted matrix according to the mass distribution of the manipulator.

The limits of the joints' range, velocity and acceleration must be considered in path planning. Let q_{l} and q_{u} denote the lower and upper limits of the joints' range, $\dot{q}_{\mathrm{l}}$ and $\dot{q}_{\mathrm{u}}$ denote the lower and upper joints' velocity limits and $\ddot{q}_{\mathrm{l}}$ and $\ddot{q}_{\mathrm{u}}$ represent the lower and upper joints' acceleration limits. The available joints' range, velocity and acceleration can be converted to velocity constraints[17] as follows:

$$\frac{\ell q_l - q(t)}{\Delta t} \leq \dot{q}(t) \leq \frac{h q_u - q(t)}{\Delta t}, \tag{31}$$

$$\beta\dot{q}_l \leq \dot{q}(t) \leq \beta\dot{q}_u, \tag{32}$$

$$\dot{q}(t - \Delta t) + \Delta t \cdot \gamma\ddot{q}_l \leq \dot{q}(t) \leq \dot{q}(t - \Delta t) + \Delta t \cdot \gamma\ddot{q}_u, \tag{33}$$

where $\ell = \mathrm{diag}[\ell_1, \ldots, \ell_m]$, $h = \mathrm{diag}[h_1, \ldots, h_m]$, $\beta = \mathrm{diag}[\beta_1, \ldots, \beta_m]$ and $\gamma = \mathrm{diag}[\gamma_1, \ldots, \gamma_m]$ $(0 < \ell_i \leq 1,$

Table I. The parameters of the OMMS service robot.

Parameter	Value (unit)	Description
$m_{l1}, \ldots, m_{l7}$	[2.7, 2.472, 2.376, 2.304, 1.536, 1.08, 0.768] (kg)	The mass of the left arm links
$m_{r1}, \ldots, m_{r7}$	[2.7, 2.472, 2.376, 2.304, 1.536, 1.08, 0.768] (kg)	The mass of the right arm links
$m_{w1}, m_{w2}, m_{w3}, m_t$	[1.6, 1.6, 1.6, 60] (kg)	The mass of the wheels and the trunk
$I_{l1}, \ldots, I_{l7}$	diag(0.019, 0.019, 0.0076), diag(0.0223, 0.0223, 0.01)	The mass moment of inertia for left and right arm links
$(I_{r1}, \ldots, I_{r7})$	diag(0.0182, 0.0182, 0.0096), diag(0.0167, 0.0167, 0.0093) diag(0.0082, 0.0082, 0.0062), diag(0.0023, 0.0023, 0.0044) diag(0.0013, 0.0013, 0.0019) (kg × m^2)	
$I_{wi}\,(i=1,2,3),\ I_t$	diag(0.0017, 0.0017, 0.0031), diag(8.55, 8.55, 2.70)(kg × m^2)	The mass moment of inertia for wheel and trunk
${}^L q_l$	[−180; 0; −45; −150; −120; −75; −60] (degree)	The low joint range limit of left arm
${}^L q_h$	[30;120; 45; 0; 90;75;60] (degree)	The high joint range limit of left arm
${}^L q_l$	[30; −120; −45; 0; −90; −75; −60] (degree)	The low joint range limit of right arm
${}^L q_h$	[180; 0; 45; 150; 120; 75; 60] (degree)	The high joint range limit of right arm
${}^L\dot{q}_{h(l)}$ (${}^R\dot{q}_{h(l)}$)	±[2;2;2;3;2.5;2.5;2.5] (grad/s)	The joint velocity limit of left arm
${}^L\ddot{q}_{h(l)}$ (${}^R\ddot{q}_{h(l)}$)	±[2;2;2;2.5;1;1;1] (grad/s^2)	The joint acceleration limit of left arm
$\dot{q}_w$	±8 (grad/s)	The rotation velocity limit of wheel
$\ddot{q}_w$	±5(grad/s^2)	The wheel rotation acceleration limit
$\xi_{l1}, \ldots, \xi_{l7}$	$[-0.495, 0, 0, 0, 1, 0]^T$, $[0, -0.495, 0, 1, 0, 0]^T$, $[0, 0, 0, 0, 0, -1]^T$,	The initial twists of the left arm joint, which is defined in the L coordinate frame
	$[-0.225, 0, 0.03, 0, 1, 0]^T$, $[0, 0, 0, 0, 0, -1]^T$, $[0, 0, 0, 1, 0, 0]^T$, $[0, 0, 0, 0, -1, 0]^T$	The initial twists of the right arm joint, which is defined in the R coordinate frame
$\xi_{l1}, \ldots, \xi_{l7}$	$[0.495, 0, 0, 0, -1, 0]^T$, $[0, 0.495, 0, 1, 0, 0]^T$, $[0, 0, 0, 0, 0, -1]^T$, $[0.225, 0, -0.03, 0, -1, 0]^T$, $[0, 0, 0, 0, 0, -1]^T$, $[0, 0, 0, 1, 0, 0]^T$, $[0, 0, 0, 0, 1, 0]^T$	
$\xi_{w1}, \xi_{w2}, \xi_{w3}$	$[0, 0, 0, 1, 0, 0]^T$, $[0, 0, 0, -0.5, 0.866, 0]^T$, $[0, 0, 0, -0.5, -0.866, 0]^T$	The initial twists of the wheels' rotation axis in the frame C
$g_{cl}(0)$, $g_{cr}(0)$	$\begin{bmatrix} 0.9397 & 0.342 & 0 & 0.0748 \\ -0.342 & 0.9397 & 0 & 0.2055 \\ 0 & 0 & 1 & 0.3795 \\ 0 & 0 & 0 & 1 \end{bmatrix}$, $\begin{bmatrix} 0.9397 & -0.342 & 0 & 0.0748 \\ 0.342 & 0.9397 & 0 & -0.2055 \\ 0 & 0 & 1 & 0.3795 \\ 0 & 0 & 0 & 1 \end{bmatrix}$	The initial configuration of the frames L and R with respect to the trunk fixed frame C

$0 < h_i \le 1,\ 0 < \beta_i \le 1,\ 0 < \gamma_i \le 1$). The joint torque limits can be indirectly realized by adjusting γ and replacing $\ddot{q}_{\mathrm{l}}$ and $\ddot{q}_{\mathrm{u}}$ with the on-line minimum and maximum acceleration output under the joint torque limits. We can combine (31), (32) and (33) to a matrix form as (30); then A and B for joint velocity constraints have the form

$$A_{\mathrm{J}} = \begin{bmatrix} -I_m \\ I_m \end{bmatrix}_{2m\times m}, \tag{34}$$

$$B_{\mathrm{J}} = \begin{bmatrix} -\max\left(\frac{\ell q_l - q(t)}{\Delta t}, \beta\dot{q}_l, \dot{q}(t-\Delta t) + \Delta t\cdot\gamma\ddot{q}_l\right) \\ \min\left(\frac{h q_u - q(t)}{\Delta t}, \beta\dot{q}_u, \dot{q}(t-\Delta t) + \Delta t\cdot\gamma\ddot{q}_u\right) \end{bmatrix}_{2m\times 1}. \tag{35}$$

In (27), we have modelled the tip-over avoidance requirement as a group inequality constraint with the form of constraint (30). Combining (27), (34) and (35), the available tip-over avoidant range of the velocity space was formed. When there is at least one solution in the range for constraint (29), the optimized algorithm expressed with (28), (29) and (30) will be effective in path planning for the OMMS system.

We will observe the discontinuity phenomenon in joint velocity when the TPC is suddenly applied into (30). In the robot moving process, sustaining efforts must be taken to avoid tip-over. At the same time, the high-level mission must be planned again when the TPC is violated. Let vector $u = [u_1 \cdots u_s]^T \in R^{s\times 1}$ be

$$u = A_T\dot{q} - B_T, \tag{36}$$

where $A_T = [({}^1A_T)^T \cdots ({}^jA_T)^T \cdots ({}^sA_T)^T]^T \in R^{s\times m}$, $B_T = [{}^1B_T \cdots {}^jB_T \cdots {}^sB_T]^T \in R^{s\times 1}$. When the robot is stable respect to the support plane, there exists $u_j \le 0$, $j = 1, \ldots, s$. The optimization criterion (25) for improving stability level can be reconstructed as $\mathrm{Min}(\max_j(u_j))$. In fact, $\min_j(u_j) < 0$ will always exist even in a robot tip-over with respect to the support plane. Considering the property of the arithmetic and geometric mean inequality, we can construct performance functions with constraints to improve the stability level:

$$\text{Minimize } u^T u, \tag{37}$$

$$\text{Subject to } u_j \le 0, \tag{38}$$

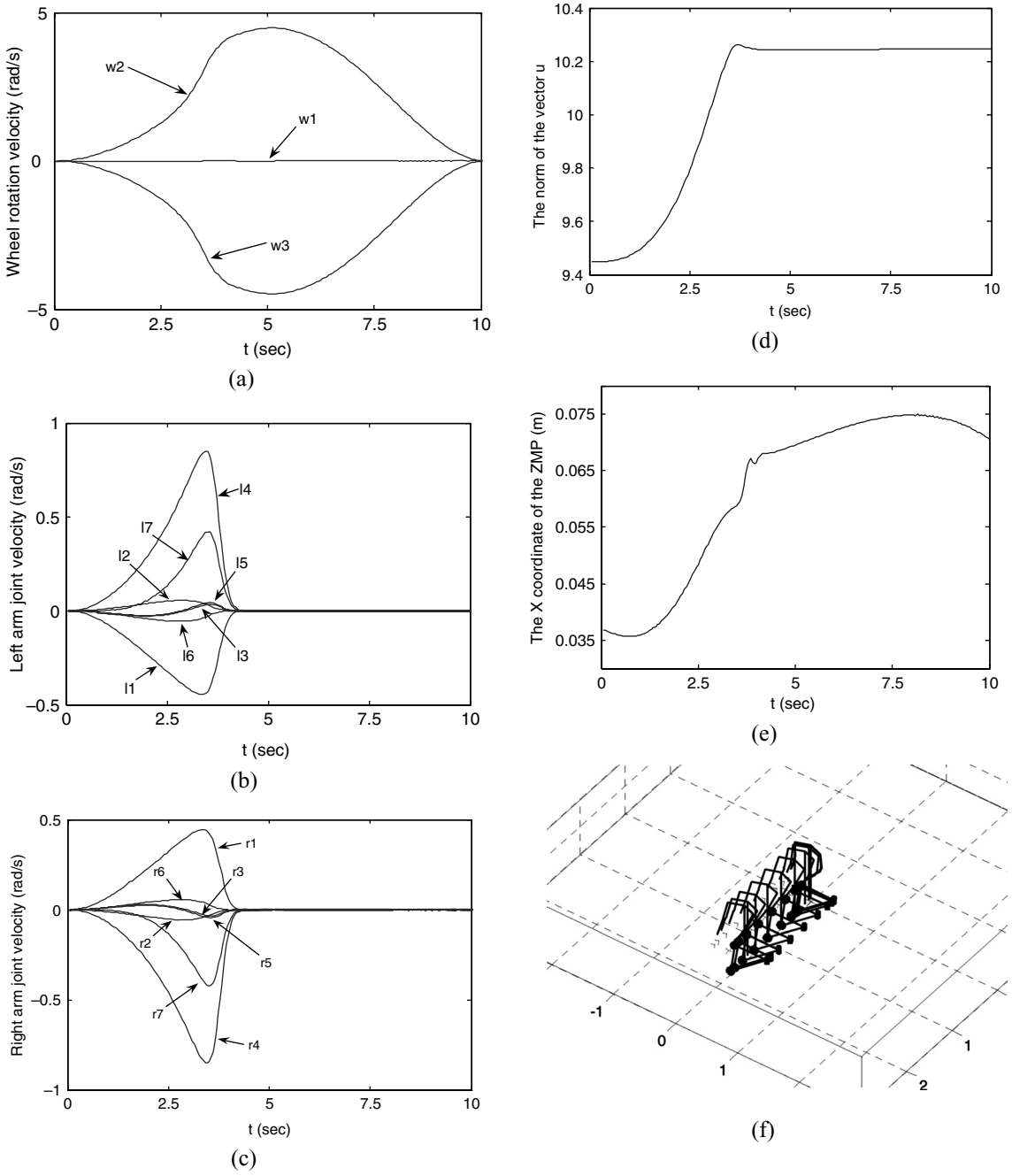

Fig. 6. Optimized solution of IRK without stability consideration and TPC for the OMMS service robot. (a) The wheel rotation velocity. (b) The left arm joint velocity. (c) The right arm joint velocity. (d) The norm of the virtual power vector u. (e) The x coordinate of the ZMP in the trunk fixed frame C. (f) The snapshot of the robot movement process.

Where the minimum of the $u^T u$ requires $\|u_i\| = \|u_j\|$. Therefore, the optimized solution of the system velocity will make sure that the ZMP be located in the geometry center of the CSP in theory.

Combining (29)–(38), the optimized solution with stability enhancing consideration for the IRK can be constructed:

$$\text{Minimize} H(q, \dot{q}) = \dot{q}^T W \dot{q} + \lambda u^T u, \tag{39}$$

$$\text{Subject to} \begin{bmatrix} J & 0 \\ A_T & -I_s \end{bmatrix} \cdot \begin{bmatrix} \dot{q} \\ u \end{bmatrix} = \begin{bmatrix} \dot{x} \\ B_T \end{bmatrix}, \tag{40}$$

$$\begin{bmatrix} A_J & 0 \\ 0 & I_s \end{bmatrix} \cdot \begin{bmatrix} \dot{q} \\ u \end{bmatrix} \leq \begin{bmatrix} B_J \\ 0_m \end{bmatrix}, \tag{41}$$

where $W \in R^{m \times m}$ is the weighted matrix and $\lambda \geq 0$ is a scalar weight which is used to adjust the tradeoff impact to the weighted energy of the robot system for tip-over prevention effort. λ will be zero when the robot is static and augments with the system kinetic energy. When one component of u approaches zero, the high-level mission re-planning algorithm must be activated to avoid the potential tip-over behaviour caused by an infeasible mission. The proposed algorithm will be verified in the next section.

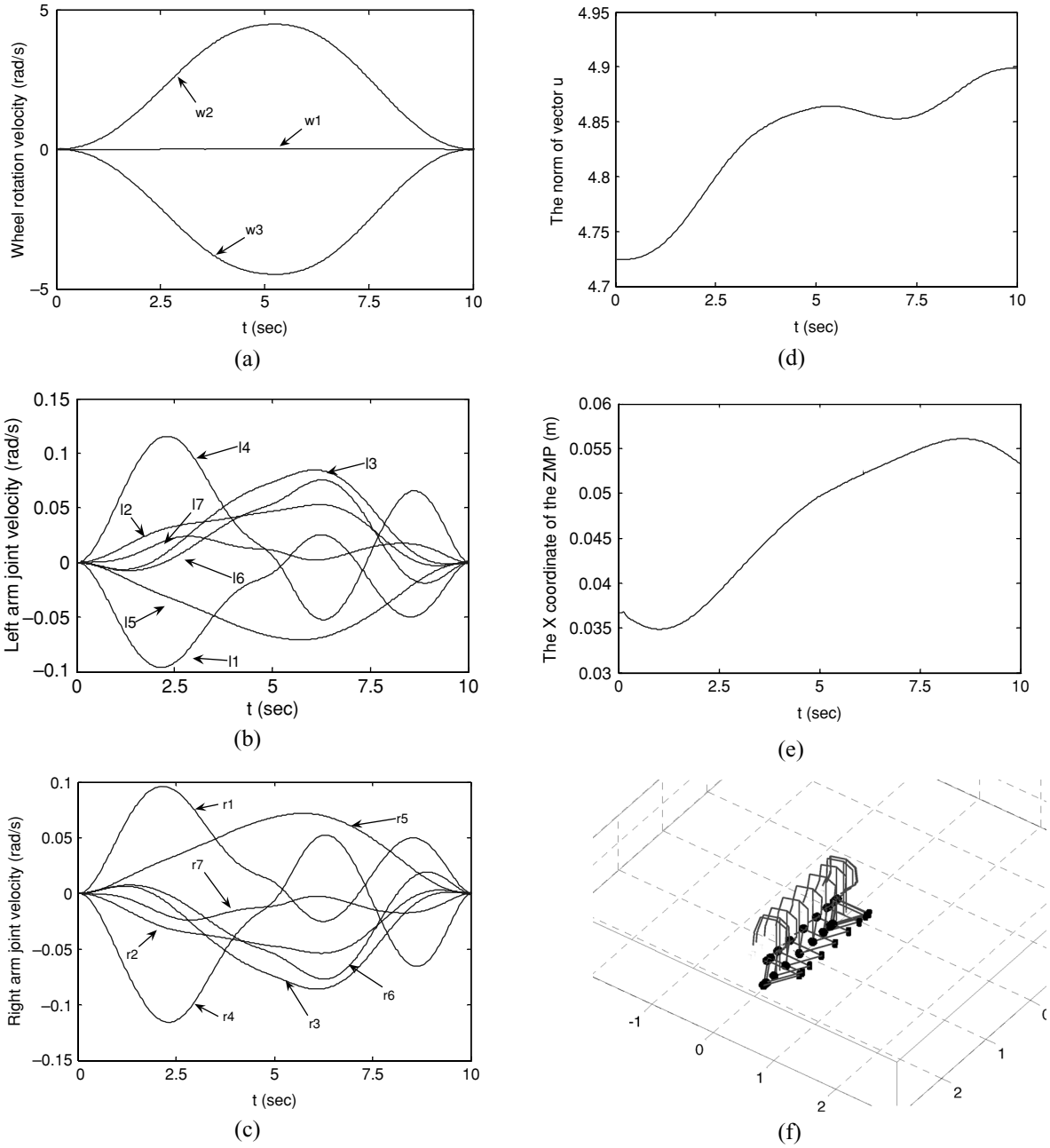

Fig. 7. Optimized solution of IRK with stability consideration and TPC for the OMMS service robot. (a) The wheel rotation velocity. (b) The left arm joint velocity. (c) The right arm joint velocity. (d) The norm of the virtual power vector u. (e) The x coordinate of the ZMP in the trunk fixed frame C. (f) The snapshot of the robot movement process.

5. Simulation Results

In order to demonstrate the effectiveness of the above methods, Matlab was used to implement the control algorithm and perform the numerical simulation for the OMMS configuration service robot movement. We presented four simulation results for comparison. The first was for the optimized solution of the IRK with only joint velocity constraints. The second was for the optimized solution with stability consideration under joint velocity and tip-over constraints. The third and fourth simulation experiments were designed to further exhibit the effectiveness of the proposed method in avoiding tip-over action. A load increased by degrees was applied on the end-effectors and the service robot's end-effectors did not change their position and pose. The improving stability level effort was considered in the fourth experiment but not in the third one. The simulation results for the four experiments are shown in Figs. 6, 7, 8 and 9, respectively. The OMMS system parameters are given in Table I.

The four simulation examples adopt the same initial parameters. The initial parameters are $q_w = [0, 0, 0]^T$, $q_l = [5^\circ, 0, 0, -90^\circ, 0, 0, -45^\circ]^T$, $q_r = [-5^\circ, 0, 0, 90^\circ, 0, 0, 45^\circ]^T$, $\ell_i = h_i = 0.95$, $\beta_i = 0.9$ and $\gamma_i = 0.9$. The initial world coordinates frame is chosen with the origin located on the support plane and the orientation of the trunk fixed frame C is I_3 with respect to the world frame W. The

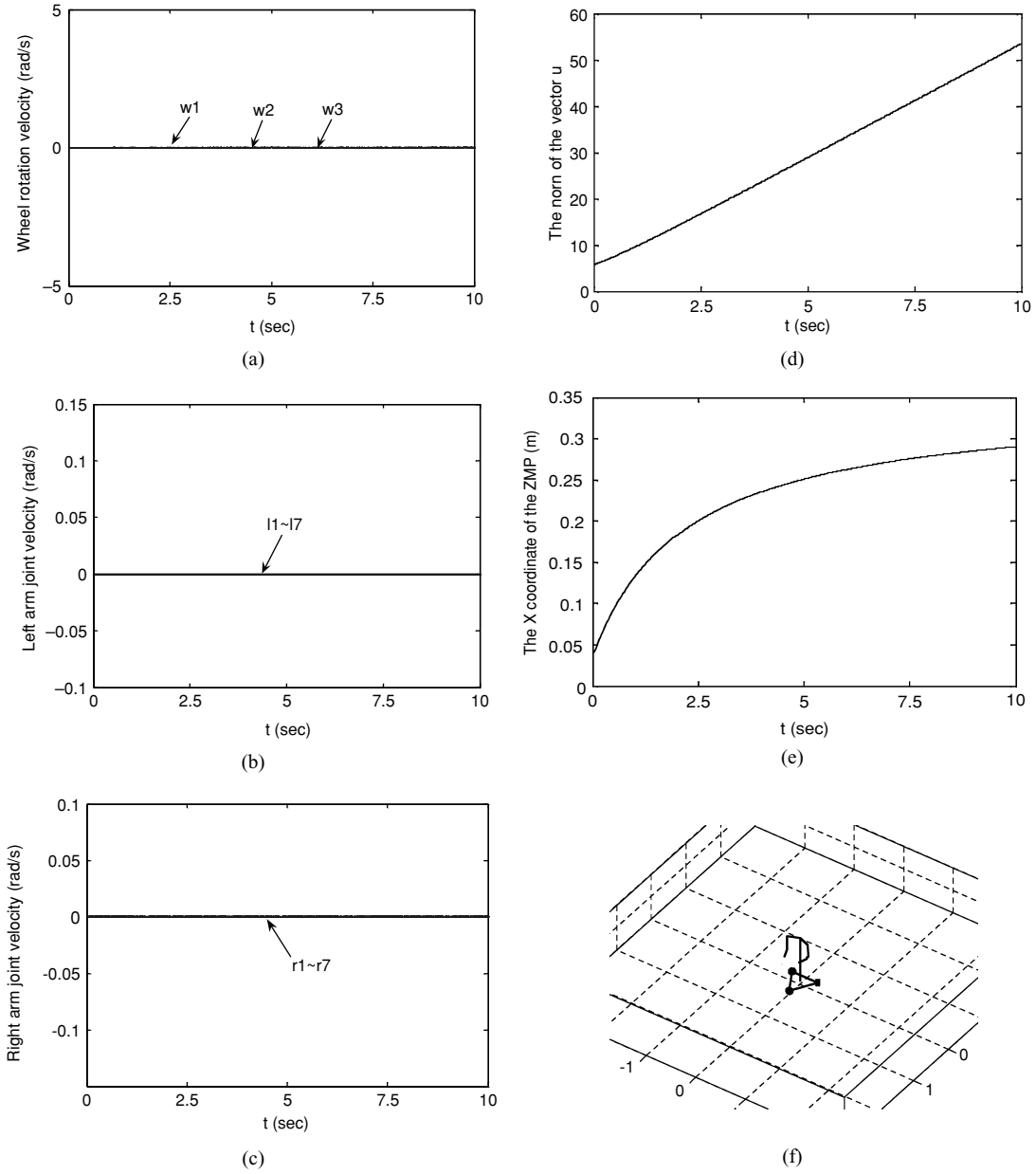

Fig. 8. Optimized solution of IRK without stability consideration and TPC for the OMMS service robot. (a) The wheel rotation velocity. (b) The left arm joint velocity. (c) The right arm joint velocity. (d) The norm of the virtual power vector u. (e) The x coordinate of the ZMP in the trunk fixed frame C. (f) The snapshot of the robot movement process.

desired path of the end-effectors for the first and second experiments is designed as moving along a straight line in $T = 10$ s from the initial position to the plane $x = 2$ and keep the end-effectors' orientation unchanged. The path is defined as $x(t) = x_0 + (x_d - x_0) \times 10(t/T)^3 - 15(t/T^4 + 6(t/T)^5)$, which has a bell-shape acceleration law. The sample time is 0.025 s. The weighted matrix in (39) is chosen as $W = \text{diag}(0.25,\ 0.25,\ 0.25,\ 2,\ 1.6,\ 1,\ 1,\ 0.8,\ 0.75,\ 0.5,\ 2,\ 1.6,\ 1,\ 1,\ 0.8,\ 0.7, 0.5) \in R^{17\times 17}$. The CSP for the two former examples was constructed with three points in the frame C; the coordinates of the points are $p_1 = [0.15, 0, -0.06]^T$, $p_2 = [-0.147, -0.2546, -0.06]^T$ and $p_3 = [-0.147, 0.2546, -0.06]^T$.

Figure 6 shows the simulation results without TPC and improving stability level consideration. The performance function is defined as the weighed joint velocity norm, and only joint motion limits (joint range, velocity and acceleration limits) are considered. In (b) and (c) of Fig. 6, we observed that the robot's arms stop movement when the mission path cannot be fulfilled by arm movement only. After that moment, the mass distribution of the whole body of the robot is not changed and only the horizontal component of the inertial force of the system is changed according to the mission. Therefore, the support force action on the virtual twists defined by the boundary of CSP will keep a constant value, which is shown in Fig. 6(d). On the other hand, the ZMP movement is decided only by the mission trajectory after that moment.

Figure 7 shows the simulation results with TPC and improving stability level consideration. The performance

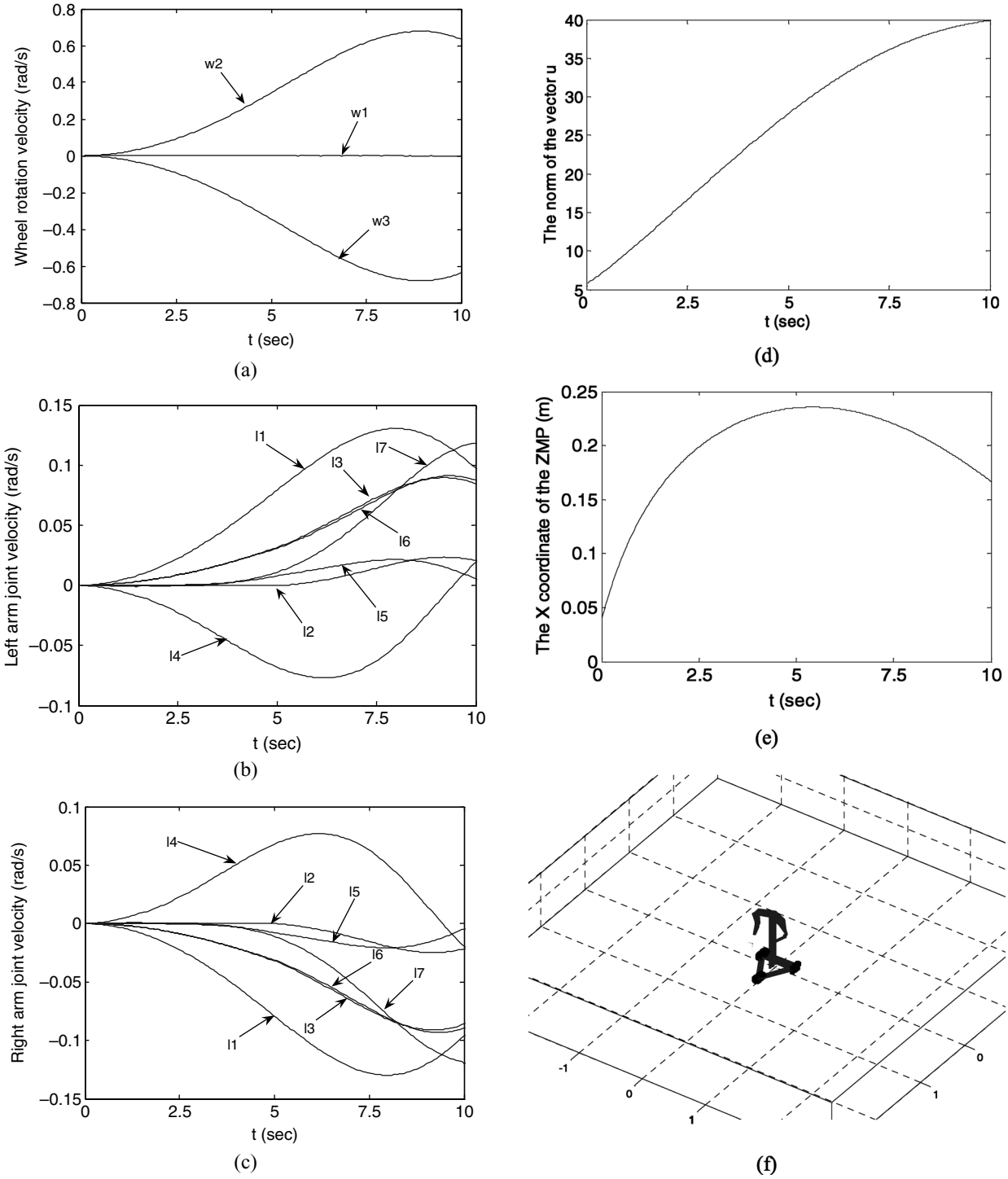

Fig. 9. Optimized solution of IRK with stability consideration and TPC for the OMMS service robot. (a) The wheel rotation velocity. (b) The left arm joint velocity. (c) The right arm joint velocity. (d) The norm of the virtual power vector u. (e) The x coordinate of the ZMP in the trunk fixed frame C. (f) The snapshot of the robot movement process.

function is defined as the sum of the weighted joint velocity norm and the weighted vector norm of u. The λ is defined as $\lambda = \lambda_m \cdot 10(|T/2 - t|/T/2)^3 - 15(|T/2 - t|/T/2)^4 + 6(|T/2 - t|/T/2)^5$, where $\lambda_m = 0.36$ and is chosen mainly considering the tradeoff with the weighted joint velocity norm by a trial-and-error process. Here, the acceleration law of the parameter, λ, is same to the mission path. In Fig. 7(b) and (c), we can find that the robot arms keep adjusting the joint velocity to fulfill the requirement of the improving stability level and finish the end-effector mission trajectory along with the wheel at the same time. The norm of the virtual power vector u shown in Fig. 7(d) is smaller than the one shown in Fig. 6(d). According to the property of the arithmetic and geometric mean inequality that the minimum value exists when non-negative variables have the same value, a smaller norm of u means that the difference of $u_j^2 (j = 1, \ldots, s)$ will be smaller. It means that the position of the ZMP will be closer to the

geometry center of the CSP. That will indirectly make the distribution of the wheels' support force more balanced when the geometry center of the CSP locates at the center of the mobile platform.

In the third and fourth experiments, we enlarge the area of the CSP by setting the point p_1 at $[0.294, 0, -0.06]^T$ in frame C; the other two vertexes of the CSP are same as in the former experiment settings. This makes all the three vertexes of the CSP be near to the supporting wheel. The load increased by degrees on end-effectors is realized by increasing the two end-effectors' gravity force with law: $F^g_{l_7(r_7)} = m_{l_7(r_7)}g + 200t$. The mass centers of the seventh link for left and right manipulators are at $[0.2903, 0.1276, 0.7039]^T$ and $[0.2903, -0.1276, 0.7039]^T$ respectively in frame C.

Figure 8 shows the experiment results without improving stability level consideration. All the joints of the robot are static because the pose and position of the end-effectors are not changed. The ZMP point moves continuously toward the supporting wheel. At time $t = 10\,s$, the ZMP approaches the point $[0.2903, 0, -0.06]^T$. It is obvious that the robot will tip-over with sustainedly increased load on end-effectors if the projection coordinates of the mass centres of the seventh link of the manipulators are outside the support polygon. In this experiment, we can find more obviously that more the ZMP moves near to the boundary of the supporting polygon, the more the norm of the virtual power vector increases. This is consistent with our analysis in Section 4.

Figure 9 shows the simulation results with improving stability level consideration. In this simulation experiment, the performance function is defined as the sum of the weighted joint velocity norm and weighted vector norm of the virtual power vector u. The λ is defined as $\lambda = 0.005t/T$ and is decided by a trial-and-error process. In Fig. 9(a–c) and (f), we can find that the robot keeps adjusting the joints' velocity to fulfill the requirement of the improving stability level and assure that the end-effectors are static. We can clearly observe the action of the improving stability method in Figs. 8(f) and 9(f). Comparing Fig. 8(d) and (e) with Fig. 9(d) and (e), it is observed that the norm of u is successfully suppressed and the ZMP is adjusted to move far away from the boundary of the support polygon. At the same time, the method presents a natural behaviour of the robot to keep support stable, which is similar to the behaviour of a human in the same situation.

On observing the simulation results presented here, we have verified the effectiveness of the proposed methods. The stability level of the robot is successfully improved. In simulation experiments, singularity avoidance must be considered in algorithm construction. We adopt the On-line Task Modification Method (OTMM)[17] to realize singularity avoidance.

6. Conclusions

Taking a service robot with OMMS configuration as a prototype for the tree topology structure mobile robot, this paper analysed the general mobile robot dynamics and dynamic stability attributes with Lie group and screw tools. The generalized stable support condition for a mobile robot is constructed not only in a polygonal support region, but also in a polyhedral support region. For a planar supporting region, the tip-over avoiding requirement is formulated as the TPC with the reciprocal products of the resultant support force screws and the imaginary tip-over twists, which are constructed with the boundaries of the support region. For alleviating the computation burden consideration, we formulate the tip-over avoiding requirement and the joint motion limits including range, velocity and acceleration limits as linear inequality constraints at velocity level. An optimized resolution algorithm with standard QP form is proposed for the inverse redundant kinematics of the mobile robot with improving stability level consideration. Simulation results demonstrated clearly the effectiveness of the proposed methods.

How to design a general adjusting method or mechanism to include the improving stability level effort into different control algorithms and kinds of missions is an open question for further study.

Acknowledgement

The work presented in this paper is supported by the 863 National High-Tech Program of China (2006AA04Z261, 2007AA041703).

References

1. E. Garcia, J. Estremera and P. Gonzalez de Santos, "A comparative study of stability margins for walking machines," *Robotica* **20**(6), 595–606 (2002).
2. E. Garcia and P. Gonzalez de Santos, "An improved energy stability margin for walking machines subject to dynamic effects," *Robotica* **23**(1), 13–20 (2005).
3. E. G. Papadopoulos and D. A. Rey, "A New Measure of Tip-Over Stability Margin for Mobile Manipulators," *Proceedings of the IEEE International Conference on Robotics and Automation*, Minneapolis, MN (Apr. 1996) pp. 3111–3116.
4. A. Ali A. Moosavian and K. Alipour, "Moment-Height Tip-Over Measure for Stability Analysis of Mobile *Robotic* Systems," *Proceedings of the IEEE International Conference on Intelligent Robots and Systems*, Beijing, China (Oct. 2006) pp. 5546–5551.
5. D. A. Rey and E. G. Papadopoulos, "On-Line Automatic Tip-over Prevention for Mobile Manipulators," *Proceedings of the IEEE International Conference on Intelligent Robots and Systems*, Grenoble, France (Sep. 1997) pp. 1273–1278.
6. R. F. Abo-Shanab and N. Sepehri, "On dynamic stability of manipulators mounted on mobile platforms," *Robotica* **19**, 439–449 (2001).
7. Q. Huang, S. Sugano and K. Tanie, "Motion Planning for a Mobile Manipulator Considering Stability and Task Constraints," *Proceedings of the IEEE International Conference on Robotics and Automation*, Leuven, Belgium (May 1998) pp. 2192–2198.
8. Y. Yamamoto and X. Yun, "Effect of the dynamic interaction on coordinated control of mobile manipulator," *IEEE Trans. Robot. Automat.* **12**(5), 816–824 (1996).
9. S. Furuno, M. Yamamoto and A. Mohri, "Trajectory Planning of Mobile Manipulator with Stability Considerations," *Proceedings of the IEEE International Conference on Robotics and Automation*, Taipei, Taiwan (Sep. 2003), pp. 3403–3408.
10. Y. Li and Y. Liu, "A New Task-Consistent Overturn Prevention Algorithm for Redundant Mobile Modular Manipulators," *Proceedings of the IEEE/RSJ International Conference on*

Intelligent Robot and Systems, Alberta, Canada (Aug. 2005), pp. 1563–1568.
11. P. B. Wieber, "On the Stability of Walking Systems," *Proceedings of the 3rd Workshop on Humanoid and Human Friendly Robots*, Tsukuba (Dec. 2002).
12. R. M. Murray, Z. Li and S. S. Sastry, *A mathematical introduction to robot manipulation* (CRC Press, Boca Raton, FL, 1993).
13. F. C. Park, J. E. Bobrow and S. R. Ploen, "A Lie group formulation of robot dynamics," *Int. J. Robot. Res.* **14**(6), 609–618 (1995).
14. M. Vukobratovi'c and B. Brovac, "Zero-moment point-thirty five years of its life," *Int. J. Humanoid Robotics* **1**(1), 157–173 (2004).
15. A. Albert and W. Gerth, "Analytic path planning algorithms for bipedal robots without a trunk," *J. Int. Robot. Syst.* **36**, 109–127 (2003).
16. Q. Huang, S. Sugano and K. Tanie, "Stability compensation of a mobile manipulator by manipulator motion: feasibility and planning," *Adv. Robot.* **13**(1), 25–40 (1999).
17. C. Qiu, Q. Cao and Y. Sun, "Resolve redundancy with constraints for obstacle and singularity avoidance subgoals," *Int. J. Robot. Automat.* **23**(1), 22–30 (2008).

Appendix: Tip-over Prevent Constraints for the OMMS System

According to (7), the inertial wrenches for the trunk, the left manipulator and the right manipulator of the OMMS system in frame C have the following forms:

$$F_C^I = M_c\dot{V}_c - ad_{V_c}^T M_c V_c, \tag{42}$$

$$\begin{aligned} {}^C F_l^I = \sum_{i=1}^{7} Ad_{g_{cl_i}^{-1}}^T \big[M_{l_i} \big(Ad_{g_{cl_i}^{-1}}\dot{V}_c + Ad_{g_{cl_i}^{-1}(0)}\,{}^l\dot{T}_{i1} V_c + J_{l_i}\ddot{q}_l \\ + \dot{J}_{l_i}\dot{q}_l \big) - ad_{V_{l_i}}^T M_{l_i} \big(Ad_{g_{cl_i}^{-1}} V_c + J_{l_i}\dot{q}_l \big) \big], \end{aligned} \tag{43}$$

$$\begin{aligned} {}^C F_r^I = \sum_{i=1}^{7} Ad_{g_{cr_i}^{-1}}^T \big[M_{r_i} \big(Ad_{g_{cr_i}^{-1}}\dot{V}_c + Ad_{g_{cr_i}^{-1}(0)}\,{}^r\dot{T}_{i1} V_c + J_{r_i}\ddot{q}_r \\ + \dot{J}_{r_i}\dot{q}_r \big) - ad_{V_{r_i}}^T M_{r_i} \big(Ad_{g_{cr_i}^{-1}} V_c + J_{r_i}\dot{q}_r \big) \big]. \end{aligned} \tag{44}$$

Substituting (42), (43) and (44) into (26), the acceleration related component in TPC has the form

$$\begin{aligned} \xi_i^T \Bigg[M_c + \sum_{i=1}^{7} Ad_{g_{cl_i}^{-1}}^T M_{l_i} Ad_{g_{cl_i}^{-1}} + \sum_{i=1}^{7} Ad_{g_{cr_i}^{-1}}^T M_{r_i} Ad_{g_{cr_i}^{-1}} \\ \times \sum_{i=1}^{7} Ad_{g_{cl_i}^{-1}}^T M_{l_i} J_{l_i} \sum_{i=1}^{7} Ad_{g_{cr_i}^{-1}}^T M_{r_i} J_{r_i} \Bigg] \begin{bmatrix} \dot{V}_c \\ \ddot{q}_l \\ \ddot{q}_r \end{bmatrix}. \end{aligned} \tag{45}$$

Applying the difference relation $\ddot{q}(t-\Delta t) = (\dot{q}(t) - \dot{q}(t-\Delta t))/\Delta t$ for $\ddot{q} = [\dot{V}_c^T \quad \ddot{q}_l^T \quad \ddot{q}_r^T]^T$, the TPC at velocity level has the form

$${}^i A_T(q(t-\Delta t))\dot{q}(t) \le {}^i B_T(q(t-\Delta t)), \tag{46}$$

where

$$\begin{cases} {}^j A_T(q(t-\Delta t)) = \xi_j^T M_s \\ {}^j B_T(q(t-\Delta t)) \\ \quad = \xi_j^T M_s \dot{q}(t-\Delta t) + \Delta t \xi_j^T (F^G + F^M) - {}^j D \\ M_s = \big[M_C + \sum_{i=1}^{7} M_{li}^C + \sum_{i=1}^{7} M_{ri}^C \sum_{i=1}^{7} Ad_{g_{c,li}^{-1}}^T M_{li} J_{li} \\ \quad \times \sum_{i=1}^{7} Ad_{g_{c,ri}^{-1}}^T M_{ri} J_{ri} \big] \\ M_{li}^C = Ad_{g_{c,li}^{-1}}^T M_{li} Ad_{g_{c,li}^{-1}} \\ M_{ri}^C = Ad_{g_{c,ri}^{-1}}^T M_{ri} Ad_{g_{c,ri}^{-1}} \\ {}^j D = \Delta t \xi_j^T \big(ad_{V_C}^T M_C V_C(t-\Delta t) + C_l + C_r \big) \\ C_l = \sum_{i=1}^{7} Ad_{g_{c,li}^{-1}}^T (M_{li}\dot{J}_{li}\dot{q}_l(t-\Delta t) \\ \quad + M_{li} Ad_{g_{c,li}^{-1}(0)}\,{}^l\dot{T}_{i1} V_c(t-\Delta t) \\ \quad - ad_{V_{li}(t-\Delta t)}^T M_{li} V_{li}(t-\Delta t)) \\ C_r = \sum_{i=1}^{7} Ad_{g_{c,ri}^{-1}}^T (M_{ri}\dot{J}_{ri}\dot{q}_r(t-\Delta t) \\ \quad + M_{ri} Ad_{g_{c,ri}^{-1}(0)}\,{}^r\dot{T}_{i1} V_c(t-\Delta t) \\ \quad - ad_{V_{ri}(t-\Delta t)}^T M_{ri} V_{ri}(t-\Delta t)) \end{cases}$$